Tetrahedron 65 (2009) 418–426

Contents lists available at ScienceDirect

Tetrahedron

journal homepage: www.elsevier.com/locate/tet

Studies on the Toxic Oil Syndrome: proposal of a mechanism for the thermal conversion of 3-*N*-phenylamino-1,2-propanediol esters into anilides under deodorisation conditions

Jordi Escabrós [a], Ramon Crehuet [b], Angel Messeguer [a,*]

[a] Department of Chemical and Biomolecular Nanotechnology, Institut de Química Avançada de Catalunya, CSIC, Barcelona, Spain
[b] Department of Biological Chemistry and Molecular Modeling, Institut de Química Avançada de Catalunya, CSIC, Barcelona, Spain

ARTICLE INFO

Article history:
Received 29 July 2008
Received in revised form
22 September 2008
Accepted 29 September 2008
Available online 10 October 2008

Keywords:
Toxic Oil Syndrome
Deodorisation
Anilides
3-*N*-Phenylamino-1,2-propanediol esters
Computational studies
Reaction mechanism

ABSTRACT

A study on the reaction mechanism for the conversion of title esters, the species recognised as toxic biomarkers of the oil batches responsible for the Toxic Oil Syndrome, into the corresponding anilides under the thermal conditions of an oil deodorisation process was performed using experimental and computational techniques. The results obtained suggest a reaction course that includes two basic steps: an intramolecular process involving the reaction of the amine group of the diester derivative with the secondary ester of the same compound, followed by the attack of an aniline molecule to form the (*E*)-isomer of an imidic acid, which would finally tautomerise to give the final anilide.

1. Introduction

Toxic Oil Syndrome (TOS) was an epidemic disease that appeared in central Spain in 1981, causing over 400 deaths and affecting more than 20,000 people.[1,2] Epidemiological data revealed that the disease was associated to the consumption of rapeseed oil denatured with aniline, illegally refined at the ITH oil refinery in Seville, mixed with others oils and sold as a grocery in an itinerant sale.[3] Several aniline derivatives were eventually detected in oil batches (Scheme 1). Fatty acid anilides were first identified (in concentrations among 500–2000 mg/L) and characterised in the suspected toxic oils.[3] However, their association with TOS was not clearly established. These fatty acid anilides were also present in adulterated oils distributed in other areas (Catalonia) with no toxicity reports among consumers[4] and they were established as adulterated toxic oil biomarkers.[3–5] Noticeably, aniline derivatives different from anilides were only found in toxic oil batches.[6] These compounds, identified as 3-(*N*-phenylamino)propane-1,2-diol (**PAP**) and its mono-, di- and triacyl derivatives[6–10] (**mPAP**, **dPAP** and **tPAP**, respectively, Scheme 1), have been subsequently considered better toxic oils biomarkers.[10] These **PAP** derivatives were not detected in the oil batches distributed in Catalonia, which suggests that something unique occurred to the aniline-denatured oils in the ITH refinery of Seville that produced the toxic oils. Unfortunately, the efforts carried out to identify the compounds that caused the intoxication have not been conclusive. In any case, the available data point to **PAP** esters or their metabolism products as

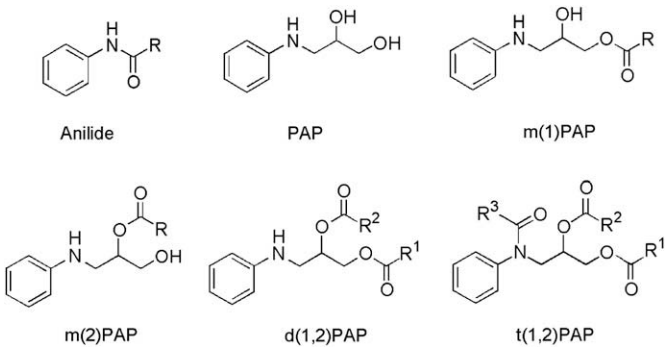

Scheme 1. Compounds associated with TOS: anilides as biomarkers of the adulterated oils and **PAP** derivatives as biomarkers of the toxic oil. R_1CO, R_2CO, and R_3CO are fatty acyl residues.

* Corresponding author. Tel.: +34 934006121.
E-mail address: angel.messeguer@iiqab.csic.es (A. Messeguer).

0040-4020/$ – see front matter © 2008 Elsevier Ltd. All rights reserved.
doi:10.1016/j.tet.2008.09.102

the most probable species responsible for eliciting the toxic effects.[11–17]

It is accepted that the agents that caused the TOS were generated during the refining of the denatured oil, in particular during the final deodorisation process. However, the chemical routes accounting for the generation of the fatty acid anilides and the different **PAP** derivatives had not been clarified. In the deodorisation step the oils are subjected to steam-distillation under vacuum to eliminate stinking compounds. During this process, abnormally high temperatures can be reached in parts of the tank, thus favouring the generation of undesired products. It is now accepted that deviations from the standard deodorisation conditions must have occurred causing the formation of **PAP** derivatives.[18] These authors observed that **PAP** esters were formed only when the oil was heated at 300 °C but not at 250 °C. Interestingly, **PAP** esters formed at 300 °C were lost during the processing at that temperature.

With these antecedents, we reproduced at a laboratory scale the deodorisation process that would have been carried out at the ITH refinery. Specifically, the production of refined aniline-denatured rapeseed oils with a composition of aniline derivatives similar to that found in the toxic oil batches was attempted.[14] This study focused on the influence of different parameters on the formation of model anilide and **PAP** derivatives from oleic acid (**OA**, **OPAP** and **OOPAP**, respectively), the interactions between any two of these variables and the occurrence of multivariable interactions. Of particular interest was the interaction observed between **OOPAP** and **OA** since these compounds have been associated to the toxic response. Specifically, we observed that the diester derivatives were unstable under the deodorisation conditions giving rise to the generation of the corresponding anilides.

The present contribution reports the study of the thermal instability of **PAP** derivatives by using both experimental and theoretical approaches. This study was addressed to propose a mechanism of such a transformation and its potential relevance to account for the toxicity effects elicited by the original oil batches.

2. Results and discussion

Our previous studies on the generation and interconversion of anilides and **PAP** derivatives during the deodorisation process showed a complex picture of transformations. Triglycerides present in the rapeseed oil containing 2% aniline reacted with this amine to give either **PAP** esters or anilides depending upon where the nucleophilic attack of aniline takes place (Scheme S1, Supplementary data). While these anilides are essentially stable under the high temperatures maintained during the deodorisation process, **PAP** esters were not, being then converted mostly into the corresponding anilides (cf. Scheme 2).[14]

This decomposition reaction should bear resemblances with the formation of amides by aminolysis of esters, a model reaction for the synthesis of peptides from amino acids in pre-biotic conditions.[19] A similar reaction is also the hydrolysis of amides, of interest when studying proteolytic enzymes.[20] Mechanism studies still disagree the intermediates involved in both reactions, but it is accepted that different paths are possible. Of special concern is the formation of the zwitterion form that arises after the initial attack of the nucleophilic species to the carboxy moiety. The results are controversial because the existence of this zwitterionic intermediate has been proved by some authors,[21,22] but questioned by others.[20] In any case, this zwitterion species should be quite unstable and would not compete with the major reaction paths. For the hydrolysis of amides, these main pathways include a proton rearrangement accompanying the C–O_{water} bond formation. Two reaction mechanisms have been postulated for this transformation. The first one is a concerted bond formation and amine elimination.

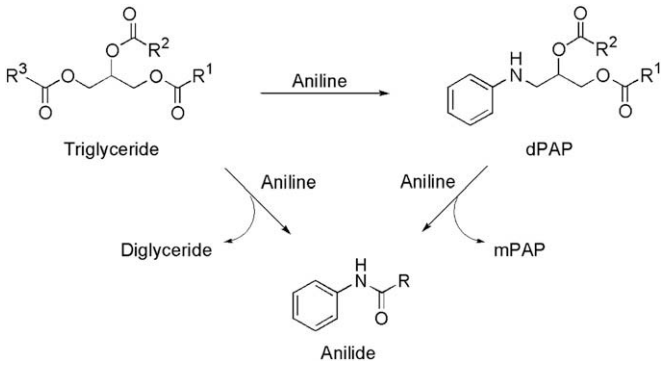

Scheme 2. Different reaction courses postulated for the nucleophilic attack of aniline on triglycerides to generate anilides or **PAP** diesters during the rapeseed oil model deodorisation process. R_1CO, R_2CO, and R_3CO are fatty acyl residues.

The second path involves a *gem*-diol intermediate: the first step consists in the addition of water followed by proton transfer to the carboxylic oxygen to give the *gem*-diol; then, this intermediate decomposes and water is released. Both mechanisms can be catalysed by water molecules that assist in the proton transfer step. Water helps by generating less strained five- and six-membered rings transition states.

The study of the decomposition of **PAP** esters resulted into a set of reaction mechanisms analogous to those described above. The peculiarity is that the functional groups involved are in the same molecule, which means that all processes are intramolecular. Another fundamental difference with aminolysis reactions is that the reactivity of **PAP** derivatives takes place in oil, a non-polar, non-protic solvent, very different from water or amines. These intramolecular transformations and an additional bimolecular mechanism will be discussed in detail to explain the formation of anilides from **PAP** derivatives.

2.1. Thermal stability studies on PAP derivatives

Although rapeseed oil is formed by a complex mixture of fatty acids and glycerides, oleic acid is the most abundant component. For this reason the oleanilide (**OA**), and the mono and dioleyl ester of **PAP** (**O(1)PAP** and **OO(1,2)PAP**, respectively) were selected to carry out part of our studies. Analogous **PAP** derivatives (**HA**, **H(1)PAP** and **HH(1,2)PAP**), containing a shorter fatty acyl residue (hexanoyl) to find out whether the length of the acid chain could influence on the thermal stability of these compounds, were also selected (Scheme 3). Finally, compounds **1**–**3** lacking one of the hydroxy moieties of **PAP** derivatives completed the set studied.

The thermogravimetry analysis profiles of some of the above compounds are shown in Figure 1. While anilide **OA** and **PAP** were thermostable until 300 °C, compounds like monoesters **O(1)PAP** and **H(1)PAP**, as well as diesters **OO(1,2)PAP** and **HH(1,2)PAP** showed two slopes (more clearly differentiated for **O(1)PAP** and **HH(1,2)PAP**), thus indicating that the thermal decomposition of the compounds took place in two stages. The first one coincides with the split of the molecule to give the corresponding anilide and the second one with the evaporation of the generated by-product. Similar results were observed for compounds **1**–**3** (Fig. 1 shows only the profile for **3**).

In another set of experiments, monoesters **O(1)PAP** and **H(1)PAP**, diester **HH(1,2)PAP**, and aminoester **3** were subjected to different constant temperatures (200, 220, 240, 260 and 280 °C) during a given period of time, and the final residue was analysed by HPLC. In all cases the respective anilides from oleic and hexanoic acid acids were detected in the assays conducted at 260 and 280 °C. Taken together, these results confirmed the observations from the

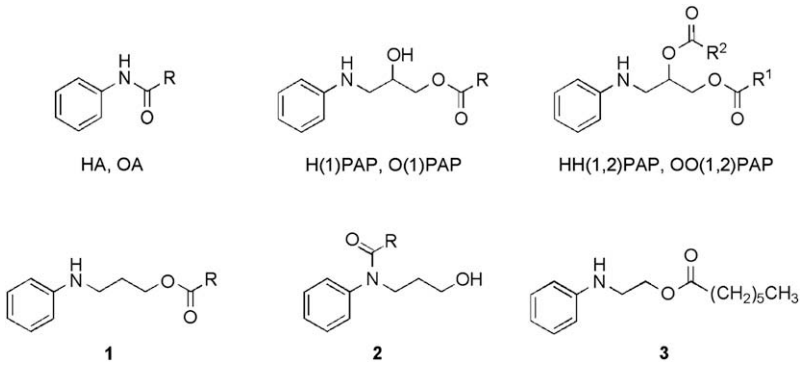

Scheme 3. Set of **PAP** derivatives and related compounds selected to analyse their thermal stability by thermogravimetry and calorimetry. **HA**: hexaneanilide; **OA**: oleanilide. In **PAP** esters fatty acyl moieties RCO are referred to hexanoyl (H) or oleyl (O) residues. Compounds **1**–**3** bear hexanoyl residues.

deodorisation process: **PAP** mono and diesters are thermally unstable giving rise to the generation of the corresponding anilides and this instability is not dependent on the length of the fatty acid chain. On the other hand, it was also observed that compound **3**, in spite of bearing a simplified structure than **PAP** derivatives, showed the same thermal behaviour, which suggested a mechanistically related pathway to account for the anilide formation. At this point we concluded that these experimental data required the support from theoretical studies.

2.2. Computational study of the thermal stability of PAP derivatives

The formation of anilides from **PAP** esters or from **3** but not from **PAP** itself deserves further analysis. In particular, we explored a reaction mechanism that could explain the formation of **OA** or **HA** from pure **PAP** esters samples under the high temperature conditions. We built a model system (see Section 4.3) where the anilides **OA** and **HA** are modelled as **5** (Scheme 4a) and the starting ester is substituted by **4**. Although precise kinetic data for the formation of anilide **5** (or **OA**, **HA**) were not available, its experimental appearance in time scale of minutes at around 530 K gives an order of magnitude for the reaction time of **4**. At a temperature of 535 K, reaction barriers of 35, 40 and 45 kcal/mol give reaction times of 0.005, 0.55, 60 h, respectively (see Section 4.3). At 555 K these rates are reduced to 0.0015, 0.13 and 12 h, respectively. These results suggest that barriers larger than 45 kcal/mol cannot explain the formation of **5** in the experimental measured times and those lower than 35 kcal/mol would result in **4** being too unstable even to be detected, in disagreement with thermogravimetry results. Therefore the reaction energy barriers that are expected lie in the range of 35–45 kcal/mol. This range can vary a few kcal/mol owing to the limitations of the quantum chemistry method used, the solvation model and the structural simplifications carried out in comparison with the real system.

Different reaction mechanisms for the decomposition of **4** have been found and some of them explain the formation of the detected product **5**. The first set of mechanisms leads to the formation of an anilide **6** with steps analogous to the aminolysis of esters. A second possible mechanism is a direct path from **4** to **5**, avoiding the anilide formation (cf. Scheme 4a). Finally, anilide **6** can suffer a nucleophilic attack from a solvent molecule to give also **5** through a bimolecular mechanism (Scheme 4b). We will see that only the energetics of the later path is in agreement with the experimental results.

2.3. Anilide 6 formation and its decomposition: TS1–TS7 (Scheme 4a and Fig. 2)

A nucleophilic attack of the amine nitrogen to the carbonyl group is a reasonable first step in the decomposition of **4**. The product of this reaction would seem to be a cyclic zwitterion. All attempts to locate the zwitterion were unsuccessful. This is in agreement with previous work showing that the zwitterion for the aminolysis of esters is highly unstable; even in water its existence is not established. [19,20] The oil used in our studies is much less polar than water; therefore, in such media, zwitterions and ionic species will be destabilised. Interestingly, two paths that are equivalent to the anilide formation in water were found, **TS1** and **TS2**+**TS3**. Anilide **6** is an intermediate of our complete reaction mechanism; it is 5.6 kcal/mol more stable than aminoester **4** and therefore it could be detected experimentally as *N*-acylated **PAP** derivative. In fact, *N*-acylated derivatives were detected in the model deodorisation experiments with doped rapeseed oil.[14] The direct path that leads to anilide **6** is **TS1**. This transition state is 58.3 kcal/mol above from **4**. This transition state has a peculiar geometry, with two five-membered rings, corresponding to the rearrangement of the acyl

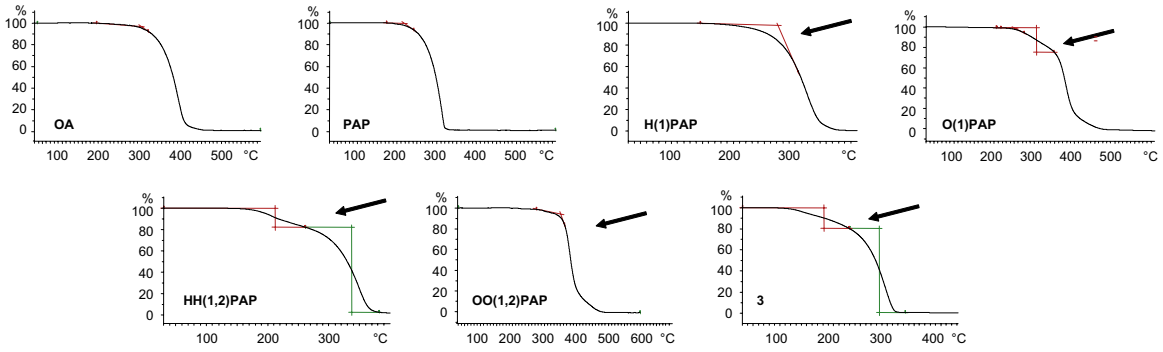

Figure 1. Thermogravimetric analysis of **OA**, **PAP**, **H(1)PAP**, **HH(1,2)PAP**, **O(1)PAP**, **OO(1,2)PAP** and compound **3**.

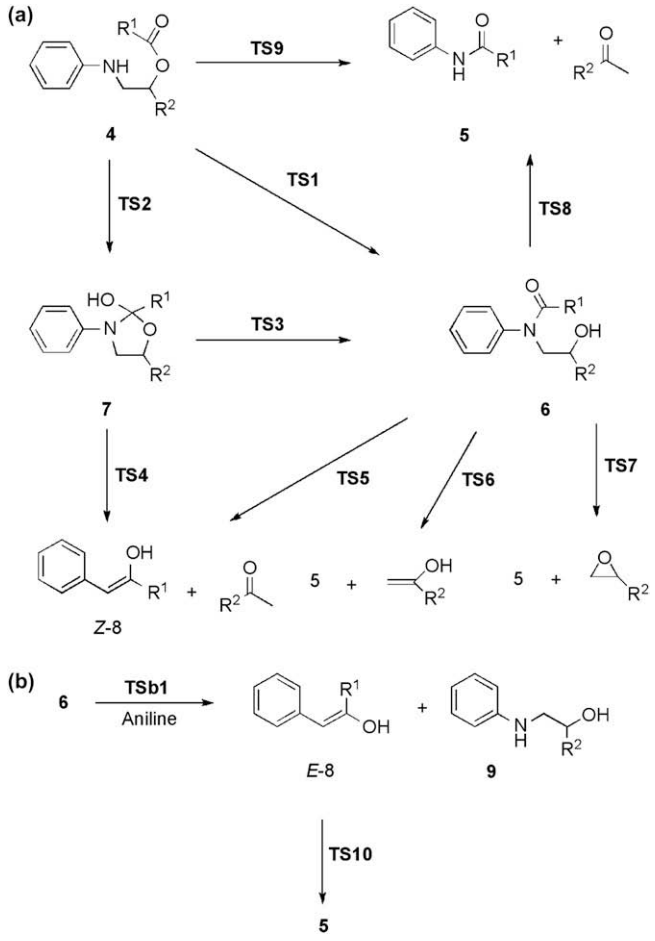

Scheme 4. Different intramolecular (a) and bimolecular (b) pathways proposed for the formation of anilide **5** from the model aminoester **4**.

and the proton in opposite directions (Fig. 2). The energy of this barrier is too high to explain the formation of **6**. Its zwitterionic character makes its solvation energy larger than that for reactants (see Table 1); however, solvation effects do not contribute substantially to its stabilisation.

A two-step process, equivalent to the *gem*-diol formation in the hydrolysis of amides was then sought. In our case, the *gem*-diol corresponds to the cyclic hemiacetal **7** (Scheme 4a). **TS2** results from the nucleophilic attack of the amine onto the carboxy moiety, but instead of giving rise to the zwitterion, a proton is concertedly rearranged in a four-membered TS to the carbonyl oxygen (Fig. 2). This TS step has a barrier of 42.6 kcal/mol; therefore intermediate **7** can be formed under the deodorisation experimental conditions. This intermediate is less stable than the reactants and its concentration will remain very small and probably beyond the sensitivity of the experimental detection methods. The formation of species **6** from **7** takes place through **TS3**. This TS has an energy higher than **TS2**. In this step, the C–O bond is broken while the proton is transferred back, again in a four-membered ring (Fig. 2). The overall path **TS2**+**TS3** has a much lower energy barrier than **TS1**.

The presence of proton donor–acceptor molecules can act as catalyst and release the strain of both **TS2** and **TS3** four-membered rings. This is a process that has been thoroughly studied with water[20,23–25] but is beyond the scope of the present work. In our system, a different molecule should play the role of water. It is conceivable that any **PAP** derivative can act as a proton donor–acceptor, as well as the carboxylic group of a fatty acid. Even if this catalytic effect takes place, it will not change the picture of the global reaction path. Indeed, the formation of **6** is the most favourable path; consequently, if catalytic effects accelerate its formation, it will remain the main intermediate along the decomposition path of aminoester **4**.

The barriers for the formation of anilide **6** are higher than those previously reported for the aminolysis of carboxylic acids.[20,22] This difference may be due to: first, the carbon atom in the ester group of **4** is less electrophilic than in a carboxylic group because the alkyl

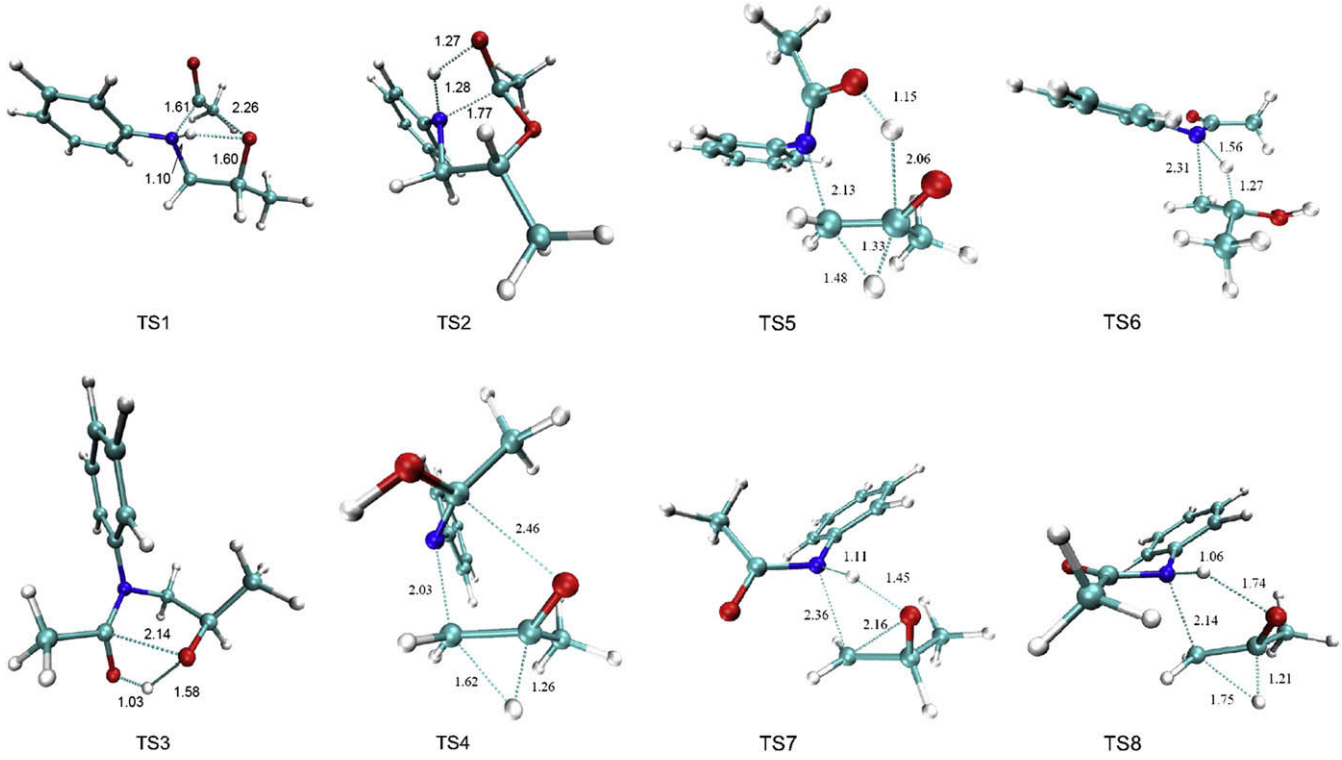

Figure 2. Transition state geometries **TS1**–**TS8** for the reaction mechanisms described in Scheme 4. Some relevant distances are depicted in angstrom.

Table 1
Energies, Gibbs free energies and solvation energies (kcal/mol) for the transition states, intermediates and products depicted in Scheme 4a

	ΔE/b2	ΔG	$\Delta\Delta G$ (solv)
4	0	0	0 (−3.6)
5+acetone	−8.5	−4.3	−1.2
5+epoxide	22.2	28.0	−0.4
5+enol	3.4	8.2	−1.0
6	−5.8	−5.6	1.5
7	11.1	17.8	0.8
E-**8**+acetone	0.8	4.9	0.2
Z-**8**+acetone	0.0	4.3	0.0
TS1	56.6	58.3	−4.1
TS2	41.6	42.6	0.7
TS3	41.8	45.2	1.1
TS4	79.6	77.6	−1.0
TS5	52.9	47.5	2.1
TS6	80.1	74.2	1.3
TS7	75.1	69.9	1.6
TS8	66.8	64.3	0.8
TS9	71.9	69.6	−1.4
TS10+acetone	31.8	33.2	0.4

substituent on the oxygen is an electron donor; second, the aniline in **4** is less nucleophilic than an amine; and last, in our study the reaction takes place in a single molecule and thus, strain features become more involved.

Postulation of intermediate **7** makes possible other reaction paths. One of them is a concerted cleavage of **7** to give acetone and an imidic acid (***Z*-8**) in its *Z* configuration, which is a tautomer of anilide **5**. The structure **TS4** corresponds to this concerted path (Fig. 2). This path is energetically very expensive and will not contribute to the reactivity of the system. The rearrangement of the formal hydride in the three-membered ring is probably the cause of such a high barrier.

The same products ***Z*-8** can be reached from anilide **6** through **TS5**. The barrier for this path is 47.5 kcal/mol. A similar TS, where the hydrogen is transferred to the nitrogen is **TS6** (Fig. 2). This TS avoids the three-membered ring strain and leads to an enol instead of acetone. Even so, its energy barrier is much higher (74.2 kcal/mol) than for **TS5**, which suggests that it is not the ring strain but the electronic redistribution the cause of such high barriers. If, instead of transferring the hydrogen attached to the carbon, it is the H of the hydroxyl that is transferred (**TS7**, Fig. 2), anilide **5** and the corresponding epoxy derivative are formed. At the transition state, the epoxide formation is concomitant with the C–N bond cleavage. As expected, the large reorganisation is accompanied by a rather high barrier for **TS7**. The last TS found for the decomposition of **6** is **TS8** (Fig. 2). For this path an energy barrier of 64.3 kcal/mol was computed. Again, it is a different combination of hydrogen transfer and bond cleavage, analogous to **TS5**, but transferring the hydrogen to the nitrogen instead of to the anilide oxygen. The high energy of these transition states combined with the fact that their geometry show a proton that is advanced in the reaction progress suggest that it is not the proton transfer that generates the energy barrier, but the cleavage of the C–N bond and the reorganisation of these electrons from the sigma to the pi system.

Taken together, after exploring exhaustively the reactivity of intermediate **6**, none of the paths can explain the generation of **5**. The reaction barriers involved are too high to be surmounted within a reasonable period of time at the working temperature range of 535–555 K reached during the deodorisation process of the model of toxic rapeseed oil.

2.4. One-step path: TS9 (Fig. 3)

As an alternative to the mechanism that gives the anilide intermediate, a concerted reaction path operating through **TS9** is also possible, affording the same products as **TS8**. **TS9** is a complex TS, where five bonds are being formed or cleaved: C–H, C–O and C–N bonds are cleaved while new C–H and C–N bonds are formed. Interestingly, the nucleophilic attack precedes all other reorganisation processes. The new C–$N_{anilide}$ bond is already formed at the TS, at a distance of 1.47 Å, and it is the separation of the anilide fragment **5** that brings a high barrier (69.9 kcal/mol). This high barriers are expected from the large number of bonds being cleaved or formed.[26] In general, a step-wise mechanism will have lower barriers and this is what is found when comparing **TS9** with the path through **TS8**. Therefore the mechanism though **TS9** is kinetically irrelevant.

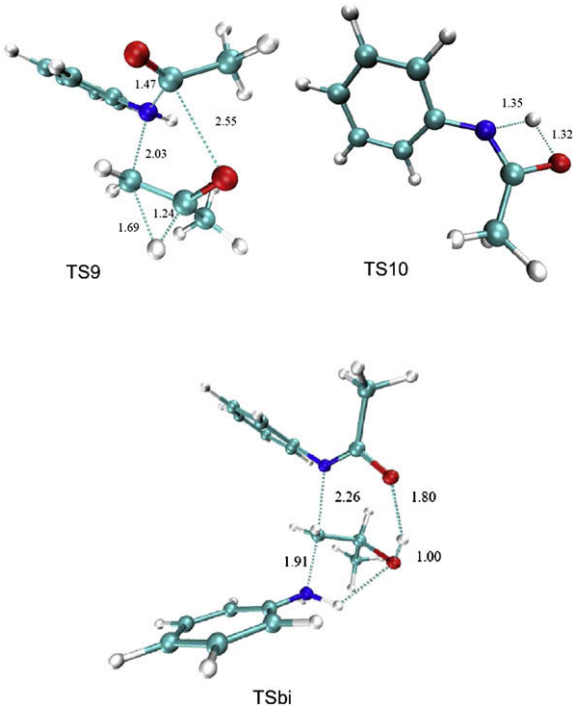

Figure 3. Transition state geometries **TS9**, **TS10**, and **TSbi** for the reaction mechanisms described in Scheme 4. Some relevant distances are depicted in angstrom.

2.5. Bimolecular mechanism

At this point, it seemed that all paths that could lead to the anilide **5** had barriers that cannot explain the fast decomposition of the starting aminoester **4** at the temperature range of the deodorisation process. All barriers appeared to be high because they involved strained transition states or they needed to cleave the C–N bond and reallocate the electrons to the π system. In other words, the amine being a good leaving group, there is no nucleophile capable to displace it directly from the carbon atom at which it is attached. It can be argued that a solvent molecule can release the strain of many of the TSs and thus catalyse the reaction. But there are two problems with this conjecture. First, none of the species present in the media is as good as a donor–acceptor as water. Even water does not usually lower the barriers from about 65 kcal/mol to 45 kcal/mol, the value that would be required for many of the transition states discussed above. Secondly, in many mechanisms it is not the proton transfer that is contributing more to the barrier but the cleavage of the C–N bond. Thus, it is difficult to envisage how a solvent molecule (in our case one of the reactants) could act on the reaction as an efficient catalyst.

As an alternative path, the elimination of an anilide **5** from intermediate **6** can be triggered by the nucleophilic attack at the

carbon atom in a S_N2 type reaction. Aniline has been selected as the most probable nucleophile present in the reaction medium, but other aniline derivatives could play the same role. The transition state **TSbi** (Scheme 4b and Fig. 3) corresponds to this process. The IRC from this transition state shows that, well after the saddle point, a proton transfer takes place form the protonated aniline to the imidate oxygen of the leaving group. Thus the product is not the anilide **5** but its tautomer, the imidic acid **8**. This acid can exist in both *Z* and *E* configurations. In this reaction, the isomer formed has the hydroxyl group in *E* conformation with respect to the nitrogen lone pair (*E*-**8**). As discussed below, this conformation makes possible a fast conversion to the anilide **5**. The energy barrier for this step is 41.3 kcal/mol.

2.6. Conversion of imidic acid to anilide

Several reaction paths discussed above yield the imidic acid **8** instead of anilide **5**. The conversion between these species is possible via a proton tautomerism. This mechanism has been studied[27,28] and can be catalysed both by acids and bases. A direct mechanism is possible if the nitrogen lone pair and the oxygen are in the cis orientation, as the result of **TSbi**. Conversely, transition states **TS4** and **TS5** lead to the trans configuration (*Z*-**8**). A trans–cis conversion has a high barrier because of the double bond character of the N–C bond. The kinetically relevant path is through **TSbi**, which gives *E*-**8**. In this molecule, the proton and the lone pair are facing the same direction and a direct path is then possible, via **TS10**. As can be seen in Figure 3, the proton is transferred along the plane while the electrons rearrange in the π system. The barrier for this process with respect to *E*-**8** is 28.9 kcal/mol and it has an exothermicity of −8.6 kcal/mol. This means that under the deodorisation experimental conditions the imidic acid *E*-**8** will rearrange to the anilide **5** without the need of the participation of a solvent molecule. This tautomerism will probably be much faster in a protic solvent. This is because the participation of a protic solvent molecule can reduce the barrier by releasing the tension of the transition state. This is a process less likely to happen in the solvent used in this work, but in any case it would result in a faster equilibration of the tautomerism. The unimolecular mechanism reported has energy barriers in agreement with other tautomeric processes involving imidic acids, such as those occurring in formamide, with a (potential energy) barrier of 33.6 kcal/mol[29] and formohydroxamic acid, with a (potential energy) barrier of around 35 kcal/mol.[30]

2.7. Six-membered ring versus five-membered ring

Because **PAP** diesters have two carboxylic groups susceptible of nucleophilic attack, two possible products can be formed. In one case it results in **7** through **TS2**. The other attack would result in a six-membered ring equivalent to **7** through **TS2′** (Scheme 5). Five- and six-membered rings have similar stability and the product distribution depends on the peculiarities of each reaction.[31] Previous experimental work in our group detected a ratio 2:1 of product yield resulting from the attack to the closer carboxylic carbon (**TS2**) with respect to the more distant one (**TS2′**).[14]

Sampling techniques to assess the flexibility of the reactant are needed to predict the product ratio, and this was done by Umbrella Sampling, as described in Section 4.3. Only **TS2** was compared because this is the initial step that decides the branching of the reaction mechanism, i.e., whether the attack gives rise to a five- or a six-membered ring (Scheme 5). It can be assumed that all the other steps for the six-membered ring will have very similar barriers as those described previously. The model used for the six-membered ring is depicted in Scheme 5.

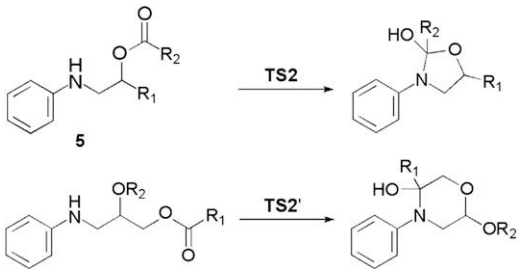

Scheme 5. Proposal for the evolution of an intermediate species via a five- or six-membered ring in the formation of anilides from **PAP** derivatives. In the calculations, R_1=R_2=CH_3.

Figure S1 illustrates the free energy profile. As expected, the conformational space for the six-membered chain is longer than the one for five-membered chain, which lowers its free energy in comparison with that of the five-membered one. This effect is, however, very small: integration of the free energy for the two basins gives only 0.3 kcal/mol of extra conformational flexibility for the six-membered ring. On the other hand, the transition state for the five-membered ring is higher in 1 kcal/mol, counteracting the effect of the entropy. The ratio in rate constants is $\exp(\Delta\Delta G^{\ddagger}/RT)$, where $\Delta\Delta G^{\ddagger}$ represents the difference in activation energies. In our case, this difference is that arising from the barrier (1 kcal/mol) minus the difference arising from the larger conformational space (0.3 kcal/mol). The result gives a rate constant for the six-membered process that is 1.9 times higher than for the five-membered, at 535 K. This is in good agreement with the experimental results in our group,[14] and it is a result of opposite entropy and enthalpy effects.

3. Conclusions

The results obtained herein have established new aspects of the chemical behaviour of several aniline derivatives during the model deodorisation process designed to imitate what occurred with the rapeseed oil batches that caused TOS intoxication. The thermal instability of **PAP** diesters due to the high temperatures achieved during the deodorisation process led to their conversion into the corresponding anilides. Therefore, **PAP** derivatives had to be considered as a new source of anilides not taken into account in previous studies.

A reaction mechanism to explain the thermal conversion of **PAP** derivatives in anilides has been established. It has been supported by theoretical studies and experimental results. This mechanism involves the combination of an intramolecular and intermolecular process. Figure 4 depicts the overall suggested reaction mechanism. First, from the **PAP** derivative, an intermediate amide **6** is formed. This intermediate is the result of the intramolecular reaction of the amino group of **PAP** derivative with the secondary ester of the same

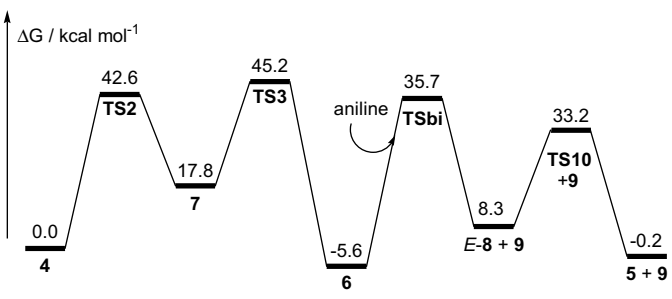

Figure 4. Overall reaction profile for the formation of **5** from **4**. Only the kinetically relevant mechanism is depicted. For other non-contributing paths, see Scheme 4 and Tables 1 and 2.

compound. Once formed, this intermediate reacts with the aniline present in the reaction medium to form the *E* isomer of an imidic acid ***E*-8**, which finally tautomerises to render the expected anilide. The formation of anilides through this mechanism explains the concomitant formation of oligomeric by-products that could remain in the insoluble resinous residues generated in the deodorisation experiments with model oil batches. This fraction was investigated in model oils without satisfactory results regarding its compound composition.[14]

Taken overall, the formation of anilides and **PAP** derivatives from aniline and triglycerides during the deodorisation process can be explained by a complex set of chemical conversions (Fig. S2, Supplementary data). In this context, the mechanistic studies described herein confirm a new path for the generation of anilides from the thermal decomposition of **PAP** esters. Interestingly, the profile shown in Figure S2 might explain the differences of toxicity observed between the Catalonian and Seville refined oils. The absence of **PAP** derivatives in Catalonian oils could be due to potential high temperatures reached during the deodorisation, which could cause the progressive decomposition of **PAP** esters present in the adulterated oil to render the corresponding anilides and by-products. These extreme thermal conditions could have been present until the complete elimination of free aniline, thus preventing the generation new of **PAP** derivatives from the reaction of the amine with triglycerides. In contrast, in the Seville oils, the deodorisation could have been carried out under not so extreme conditions, which conditioned that **PAP** esters could remain in some extent in the final refined oil.

4. Experimental section

4.1. General

Aniline, oleic acid, hexanoic acid, *N*,*N*-(dimethylamino)pyridine (DMAP) and *N*,*N*-dicyclohexylcarbodiimide (DCC) were from Aldrich, Germany. Solvents were of HPLC grade and purchased from Merck, Germany. The synthesis of **PAP**, **OPAP**, **OOPAP** and **OA** has been described elsewhere.[32] Anilide from hexanoic acid was available at the laboratory. The NMR spectra were recorded on a Varian Inova 500 (499.08 MHz for ^{1}H and 125.67 MHz for ^{13}C). Spectra were taken in neutralised $CDCl_3$ solutions unless otherwise indicated. Chemical shifts (δ) are given in parts per million relative to tetramethylsilane (^{1}H, 0.0 ppm) or $CDCl_3$ (^{13}C, 77.0 ppm). The LC/MS analyses were carried out with a Hewlett–Packard Series 1100 LC/MSD or 1090LC/1100MSD apparatus equipped with an electrospray source working in positive ion mode. The GC/MS analyses were carried out with a ThermoFinnigan Trace GC/MS apparatus equipped with an electron ionisation detector (70 eV). Analytical HPLC samples were run on an HP series 1100 system equipped with a direct-phase column (Nucleosil 100-5CN, 5 μm, 150×4 mm from Scharlau, Spain). Elution conditions: hexane/2-propanol mixtures at 1 mL/min. UV detection was set at λ=245 and 270 nm. A Biotage system (Dyax Corp., Cambridge, MA) equipped with silica gel Kpsil (32–63 μm, 60 Å) columns was employed for flash chromatography purifications. The preparative HPLC purifications were performed by semi-preparative HPLC using a Kromasil C8 (25×2 cm, 5 μm) column, CH_3CN/H_2O mixtures containing 0.1% TFA as mobile phases and a flow rate of 5 mL/min. UV detection was set at λ=220 nm. High resolution mass spectra (HRMS-FAB) were carried out at the Mass spectrometry Service of the University of Santiago de Compostela (Spain). The elemental analyses were performed at the IQAC Microanalysis Service. Thermogravimetry studies were performed with a Mettler Toledo TG50 apparatus and calorimetry studies with a DSC821 apparatus.

4.2. Synthesis of 3-(phenylamino)propyl hexanoate (1)

4.2.1. 3-(Phenylamino)propanol

Aniline (400 μl, 4.38 mmol) was added dropwise to 3-cloro-1-propanol (410 mg, 4.33 mmol). When the addition was completed, the mixture was stirred under reflux for 11 h (HPLC monitoring). The crude reaction mixture was purified by flash chromatography (9:1 Et_2O/CH_2Cl_2) to give the expected compound as a colourless oil (80 mg, 12%). ^{1}H NMR δ 7.17 (t, J=7 Hz, 2H, CH_{Ar}), 6.71 (t, J=7.5 Hz, 1H, CH_{Ar}), 6.62 (d, J=7.5 Hz, 2H, CH_{Ar}), 3.75 (t, J=6 Hz, 2H, CH_2OH), 3.23 (t, J=6.5 Hz, 2H, CH_2NHPh), 1.83 (q, J=6 Hz, 2H, CH_2CH$_2$OH). ^{13}C NMR δ 142.2 (C-1 aniline), 129.2 (C-3, C-5 aniline), 117.6 (C-4 aniline), 113.1 (C-2, C-6 aniline), 61.3 (CH_2OH), 41.8 (CH_2NHPh), 31.7 (CH_2CH$_2$OH). HRMS: m/z 152.1075; m/z for $(M+H)^+$ $C_9H_{14}NO$ requires 152.1066.

*4.2.2. 3-(Phenylamino)propyl hexanoate (**1**)*

A mixture of 3-(phenylamino)propanol (39 mg, 0.25 mmol), oleic acid (328 mg, 0.28 mmol), DCC (61 mg, 0.29 mmol) and DMAP (5 mg, 0.04 mmol) in CH_2Cl_2 (2 mL) was allowed to react at room temperature. When the reaction was completed (3 h, TLC monitoring), the solvent was evaporated to dryness and the residue obtained was dissolved in hexane to induce precipitation of the urea derivative. Purification of the crude reaction mixture by flash chromatography (silica gel, 8:1 hexane/EtOAc) afforded the expected ester **1** as a colourless oil (46 mg, 72% yield). ^{1}H NMR δ 7.17 (t, J=7.5 Hz, 2H, CH_{Ar}), 6.70 (t, J=7.5 Hz, 1H, CH_{Ar}), 6.61 (d, J=8.5 Hz, 2H, CH_{Ar}), 4.20 (t, J=6.5 Hz, 2H, CH_2OCO), 3.77 (1H, NH), 3.22 (t, J=6.5 Hz, 2H, CH_2NH), 2.32 (t, J=7.5 Hz, 2H, CH_2CO), 1.94 (q, J=6.5 Hz, 2H, CH_2CH$_2$CO), 1.63 (q, J=7.5 Hz, 2H, CH_2CH$_2$CH$_2$CO), 1.34–1.29 (4H, CH_2), 0.90 (t, J=7 Hz, 3H, CH_3). ^{13}C NMR δ 173.9 (CO), 148.0 (C-1 aniline), 129.3 (C-3, C-5 aniline), 117.4 (C-4 aniline), 112.8 (C-2, C-6 aniline), 62.1 (CH_2OCO), 40.7 (CH_2NHPh), 34.3 (CH_2CO), 31.7 (CH_2CH$_2$OH), 28.6 (CH_2), 24.7 (CH_2), 22.3 (CH_2), 13.9 (CH_3). HPLC-MS: 250.1 $(M+H)^+$. EIMS m/z (%): 249.13 (50) molecular ion, 132.04 (20), 106.04 (100), 77.03 (30). HRMS: m/z 250.1807; m/z for $(M+H)^+$ $C_{15}H_{24}NO_2$ requires 250.1826.

*4.2.3. N-Hexanoyl-3-(phenylamino)propanol (**2**)*

Hexanoyl chloride (95 μl, 0.60 mmol) and triethylamine (45 μl, 0.32 mmol) were added to a solution of 3-(phenylamino)propanol (52 mg, 0.34 mmol) in CH_2Cl_2 (1 mL) and the mixture was stirred for 1 h at 25 °C (HPLC monitoring). After the elimination of the solvent under vacuum, the residue was purified by semi-preparative HPLC eluting with 15:85 H_2O/acetonitrile to yield the expected compound (32 mg, 40% yield). ^{1}H NMR δ 7.44 (t, J=9.5 Hz, 2H, CH_{Ar}), 7.38 (t, J=7.5 Hz, 1H, CH_{Ar}), 7.14 (d, J=4.5 Hz, 2H, CH_{Ar}), 3.87 (t, J=6.0 Hz, 2H, CH_2OH), 3.65 (2H, CH_2NCO), 2.05 (t, J=7.5 Hz, 2H, CH_2CO), 1.66 (qu, J=5.5 Hz, 2H, CH_2CH$_2$CON), 1.57 (qu, J=7.5 Hz, 2H, CH_2CH$_2$OH), 1.25–1.14 (4H, CH_2CH_2CH$_2$CH$_2$CON), 0.83 (t, J=7 Hz, 3H, CH_3). ^{13}C NMR δ 174.8 (CO), 142.0 (C-1 aniline), 129.9 (C-3, C-5 aniline), 128.1 (C-4 aniline), 128.0 (C-2, C-6 aniline), 58.1 (CH_2OH), 45.6 (CH_2NH), 34.1 (CH_2CON), 31.3 (CH_2CH$_2$OH), 29.9 (CH_2), 25.2 (CH_2), 22.3 (CH_2), 13.9 (CH_3). HPLC-MS: 521.5 $(M+M+Na)^+$, 272.2 $(M+Na)^+$, 250.2 $(M+H)^+$. HRMS: m/z 250.1807; m/z for $(M+H)^+$ $C_{15}H_{24}NO_2$ requires 250.1822.

*4.2.4. 2-(Phenylamino)ethyl hexanoate (**3**)*

A mixture of 2-(phenylamino)ethanol (200 mg, 1.46 mmol), hexanoic acid (180 mg, 1.55 mmol), DCC (332 mg, 1.61 mmol) and DMAP (16 mg, 0.13 mmol) in CH_2Cl_2 (4 mL) was allowed to react at room temperature. When the reaction was complete (3 h, HPLC monitoring), working-up and purification of the crude reaction mixture as described above for **1** afforded pure **5** (273 mg, 80% yield). ^{1}H NMR δ 7.19 (t, J=7.5 Hz, 2H, CH_{Ar}), 6.73 (t, J=7.5 Hz, 1H, CH_{Ar}), 6.64 (d, J=7.5 Hz, 2H, CH_{Ar}), 4.29 (t, J=5.5 Hz, 2H, CHHOR), 3.89 (s, 1H, CNH_{Ar}), 3.40 (q, J=5.5 Hz, 2H, CHHN), 2.32 (t, J=7.5 Hz,

2H, $COCH_2$), 1.60–1.64 (2H, $COCH_2CH_2$), 1.40–1.20 (4H, CH_2), 0.88 (t, J=6.5 Hz, 3H, CH_3). ^{13}C NMR δ 173.9 (CO), 147.6 (CH_{Ar}), 129.3 ($2CH_{Ar}$), 117.8 (CH_{Ar}), 112.9 ($2CH_{Ar}$), 62.8 (CH_2OCOR), 42.9 (CH_2NH), 34.1 (CH_2), 31.3 (CH_2), 24.6 (CH_2), 22.3 (CH_2), 13.9 (CH_3). Anal. Calcd for $C_{14}H_{21}NO_2$: C, 71.46%; H, 8.99%; N, 5.95%. Found: C, 71.49%; H, 9.15%; N, 6.13%.

4.3. Computational details

The aim of the computational work is to derive a mechanism for the formation of anilides **HA** and **OA** from **PAP** derivatives such as **m(2)PAP** or **PAP** analogues such as **3** (see Section 2). Because the length of substituents was not relevant for the formation of the anilides, aminoester **4** was selected as model **PAP** surrogate, and R_1 and R_2 were chosen as methyl groups.

All calculations were done based on the Density Functional Theory, using the hybrid functional B3LYP.[33] Stationary points were located and characterised with frequency calculations. We checked that minima had all positive frequencies and that Transition States (TSs) had only one imaginary frequency. To prove that each TS connected with the reactants and products, the Intrinsic Reaction Coordinate (IRC) was followed. The basis set used for the optimisation was 6-31G(d), which we will refer as b1. To get more reliable energies, single point calculations on the optimised geometries with 6-311+G(d,p) were carried out. This triple-zeta basis set will be referred as b2. Enthalpy and free energy corrections to the b2 basis set were calculated with the thermochemistry results at B3LYP/b1 at 533 K. This seems reasonable since the energy results did not differ significantly with both basis sets (see Tables 1 and 2, and Tables S1 and S2), thus indicating that potential energy surfaces described with the different basis are very similar. All these calculations were performed with the PC GAMESS program.[34]

Table 2
Energies, Gibbs free energies and solvation energies (kcal/mol) for the transition states, intermediates and products depicted in Scheme 4b

	ΔE/b2	ΔG	$\Delta\Delta G$ (solv)
6+aniline	0	0	0 (−5.4)
TSbi	49.7	41.3	0.7
E-**8**+**9**	12.0	13.9	−1.1

The environment effects were included with a polarisable continuum model, PCM.[35] Because the olive oil or the oleic acid had not been parametrised, we used diethylether as solvent, which has similar dielectric properties. As results are not significantly changed by the solvent, its replacement is an acceptable approximation. Solvation effects were calculated at 300 K because the parameters for diethylether are not available at 500 K (where it is no longer a liquid). Again, because solvent effects are small and the energy differences between mechanisms large, the temperature changes should not be significant. PCM calculations were performed with Gaussian 98.[36] Throughout the results, when discussing energy barriers and exothermicity data, we will refer to free energy values in vacuum unless otherwise stated.

Transition State Theory (TST) was used to calculate rate constants. Harmonic partition functions were used and no translational or rotational effects were included because they are only meaningful in gas-phase. The reaction time was defined as the inverse of the rate constant, $k(T)$. TST expression of the reaction rate constant is expressed as Eq. 1, where h is the Planck constant, T the temperature, k_B the Boltzmann constant, R the gas constant and ΔG the activation free energy.

$$k(T) = \frac{k_B T}{h}\exp\left(\frac{\Delta G}{RT}\right) \quad (1)$$

Potentials of mean force were calculated with the Umbrella Sampling method combined with the Weighted Histogram Analysis Method.[37,38] Due to the high computational cost of the molecular dynamics simulations needed for this technique, the semi-empirical Hamiltonian AM1 was used. This should be reliable enough because only energy differences for the same mechanism were compared. These calculations were performed with the DYNAMO suite of subroutines.[39,40] As a reaction coordinate (rc) to build the free energy profile or potential of mean force, the following combination of distances was used rc=d(C–N)+d(H–O)−d(H–N).

Acknowledgements

This work was supported by FISAT-WHO Grants. We thank Josep Carilla for the thermogravimetry measurements, J.M. Anglada for fruitful discussions and J. Luque for helpful hints in solvation calculations. R.C. would like to thank the Ramón y Cajal program of the Spanish government and MEC for financial support (Grant CTQ2006-01345/BQU). This research has been partly performed using the CESCA resources.

Supplementary data

Schemes S1 and S2 containing more details of reaction mechanisms; Figure S1, depicting the free energy profile for the bimolecular mechanism; Tables S1 and S2, complementing Tables 1 and 2, are provided. Supplementary data associated with this article can be found in the online version, at doi:10.1016/j.tet.2008.09.102.

References and notes

1. Posada de la Paz, M.; Philen, R. M.; Abaitua Borda, I. *Epidemiol. Rev.* **2001**, *23*, 231–247.
2. Diggle, G. E. *Int. J. Clin. Pract.* **2001**, *55*, 371–375.
3. Pestaña, A.; Muñoz, E. *Nature* **1982**, *298*, 608.
4. Ventura Díaz, L. M. *Grasas y Aceites* **1982**, *33*, 73–78.
5. Gradjean, P.; Tarkowski, S. *Toxic Oil Syndrome. Mass Food Poisoning in Spain.* WHO Regional Office for Europe: Copenhagen, Denmark, 1984, pp 3–16.
6. Vázquez-Roncero, A.; Janer del Valle, C.; Maestro Durán, R.; Graciani Constante, E. *Lancet* **1983**, *ii*, 1024–1025.
7. Vázquez-Roncero, A.; Maestro Durán, R.; Gutiérrez, R. *Grasas y Aceites* **1984**, *35*, 15–21.
8. Vázquez Roncero, A.; Gómez Gómez, R. *Grasas y Aceites* **1987**, *38*, 87–92.
9. Posada de la Paz, M.; Philen, R. M.; Schurz, H.; Hill, R. H. J.; Giménez Ribota, O.; Gómez de la Cámara, A.; Kilbourne, E. M.; Abaitua Borda, I. *Epidemiology* **1999**, *10*, 130–134.
10. Schurz, H. H.; Hill, R. H.; Posada de la Paz, M.; Philen, R. M.; Borda, I. A.; Bailey, S. L.; Needham, L. L. *Chem. Res. Toxicol.* **1996**, *9*, 1001–1006.
11. Ladona, M. G.; Bujons, J.; Messeguer, A.; Ampurdanés, C.; Morató, A.; Corbella, J. *Chem. Res. Toxicol.* **1999**, *12*, 1127–1137.
12. Bujons, J.; Ladona, M. G.; Messeguer, A.; Morató, A.; Ampurdanés, C. *Chem. Res. Toxicol.* **2001**, *14*, 1097–1106.
13. Morató, A.; Martínez-Cabot, A.; Escabrós, J.; Bujons, J.; Messeguer, A. *Chem. Res. Toxicol.* **2004**, *17*, 889–895.
14. Morató, A.; Escabrós, J.; Manich, A.; Reig, N.; Castaño, Y.; Abian, J.; Messeguer, A. *Chem. Res. Toxicol.* **2005**, *18*, 665–674.
15. Martínez-Cabot, A.; Morató, A.; Messeguer, A. *Chem. Res. Toxicol.* **2005**, *18*, 1721–1728.
16. Martinez-Cabot, A.; Messeguer, A. *Chem. Res. Toxicol.* **2007**, *20*, 1556–1562.
17. Reig, N.; Calaf, R. E.; Castaño, Y.; Prieto, R.; Messeguer, A.; Morató, A.; Escabrós, J.; Gelpí, E.; Abian, J. *J. Mass Spectrom.* **2007**, *42*, 527–541.
18. Ruíz-Méndez, M. V.; Posada de la Paz, M.; Abian, J.; Calaf, R. E.; Blount, B.; Castro-Molero, N.; Philen, R.; Gelpí, E. *Food Chem. Toxicol.* **2001**, *39*, 91–96.
19. Chalmet, S.; Harb, W.; Ruiz-López, M. F. *J. Phys. Chem.* **2001**, *105*, 11574–11581.
20. Gorb, L.; Asensio, A.; Tuñón, I.; Ruiz-López, M. F. *Chem.—Eur. J.* **2005**, *11*, 6743–6753.
21. Cascella, M.; Raugei, S.; Carloni, P. *J. Phys. Chem. B* **2004**, *108*, 369–375.
22. Zahn, D. *Eur. J. Org. Chem.* **2004**, *69*, 4020–4023.
23. Crehuet, R.; Anglada, J. M.; Bofill, J. M. *Chem.—Eur. J.* **2001**, *7*, 2227–2235.
24. Anglada, J. M.; Aplincourt, P.; Bofill, J. M.; Cremer, D. *ChemPhysChem* **2002**, *2*, 215–221.
25. Aplincourt, P.; Anglada, J. M. *J. Phys. Chem.* **2003**, *107*, 5812–5820.
26. Dewar, M. J. S. *J. Am. Chem. Soc.* **1984**, *106*, 209–219.
27. Eriksson, M. A.; Hard, T.; Nilsson, L. *Biophys. J.* **1995**, *69*, 329–339.

28. Ciarkowski, J.; Chen, F. M. F.; Benoiton, N. L. *J. Comput.-Aided Mol. Des.* **1991**, *5*, 599–616.
29. Adamo, C.; Cossi, M.; Barone, V. *J. Comput. Chem.* **1997**, *18*, 1993–2001.
30. Hwa, D.-H.; Ho, J.-J. *J. Phys. Chem.* **1998**, *102*, 3582–3586.
31. Carey, F. A.; Sundberg, R. J. *Advanced Organic Chemistry: Structure and Mechanisms.* Plenum: New York, NY USA, 2000.
32. Ferrer, M.; Galceran, M.; Sánchez-Baeza, F.; Casas, J.; Messeguer, A. *Liebigs Ann. Chem.* **1993**, 507–511.
33. Becke, A. M. *J. Chem. Phys.* **1993**, *98*, 5648–5652.
34. Granovsky, A. A. PC GAMESS version 7.0, http://classic.chem.msu.su/gran/gamess/index.html.
35. Tomasi, J.; Mennucci, B.; Cammi, R. *Chem. Rev.* **2005**, *105*, 2999–3094.
36. Frisch, M. J.; Trucks, G. W.; Schlegel, H. B.; Scuseria, G. E.; Robb, M. A.; Cheeseman, J. R.; Montgomery, Jr., J. A.; Vreven, T.; Kudin, K. N.; Burant, J. C.; Millam, J. M.; Iyengar, S. S.; Tomasi, J.; Barone, V.; Mennucci, B.; Cossi, M.; Scalmani, G.; Rega, N.; Petersson, G. A.; Nakatsuji, H.; Hada, M.; Ehara, M.; Toyota, K.; Fukuda, R.; Hasegawa, J.; Ishida, M.; Nakajima, T.; Honda, Y.; Kitao, O.; Nakai, H.; Klene, M.; Li, X.; Knox, J. E.; Hratchian, H. P.; Cross, J. B.; Bakken, V.; Adamo, C.; Jaramillo, J.; Gomperts, R.; Stratmann, R. E.; Yazyev, O.; Austin, A. J.; Cammi, R.; Pomelli, C.; Ochterski, J. W.; Ayala, P. Y.; Morokuma, K.; Voth, G. A.; Salvador, P.; Dannenberg, J. J.; Zakrzewski, V. G.; Dapprich, S.; Daniels, A. D.; Strain, M. C.; Farkas, O.; Malick, D. K.; Rabuck, A. D.; Raghavachari, K.; Foresman, J. B.; Ortiz, J. V.; Cui, Q.; Baboul, A. G.; Clifford, S.; Cioslowski, J.; Stefanov, B. B.; Liu, G.; Liashenko, A.; Piskorz, P.; Komaromi, I.; Martin, R. L.; Fox, D. J.; Keith, T.; Al-Laham, M. A.; Peng, C. Y.; Nanayakkara, A.; Challacombe, M.; Gill, P. M. W.; Johnson, B.; Chen, W.; Wong, M. W.; Gonzalez, C.; Pople, J. A. *Gaussian 03. Revision C.02*. Gaussian: Wallingford, CT, USA.
37. Kumar, S.; Rosenberg, J. M.; Bouzida, D.; Swendsen, R. H.; Kollman, P. A. *J. Comput. Chem.* **1992**, *13*, 1011–1021.
38. Roux, B. *Comput. Phys. Commun.* **1995**, *91*, 275–282.
39. Field, M. J.; Céline, M. A.; Proust-De, B. F.; Thomas, M. A. *J. Comput. Chem.* **2000**, *21*, 1088–1100.
40. Field, M. J. *A Practical Introduction to the Simulation of Molecular Systems*; Cambridge University Press, Cambridge, UK, 1999.